Direct Bi 3+ -Bi 3+ contacts mediated by lonepairs in the HP-BiNiO(PO4) polymorph

Marie Colmont, Anastasiya Zadoya, Céline Darie, Cyril Domingos, Bastien Leclercq, Olivier Mentré

Direct Bi^{3+}-Bi^{3+} contacts mediated by lonepairs in the HP-$BiNiO(PO_4)$ polymorph

Marie Colmont,[1*] Anastasiia Zadoya,[1] Céline Darie,[2] Cyril Domingos, [2]Bastien Leclercq,[1] and Olivier Mentré[1]

[1] Université Lille, CNRS, Centrale Lille, ENSCL, Université Artois, UMR 8181, Unité de Catalyse et Chimie du Solide, Lille, F-59000, France.

[2] Université Grenoble Alpes et CNRS, Institut NEEL, F-38042 Grenoble, France

Supporting Information Placeholder

ABSTRACT: A high-pressure polymorph of $BiNiPO_5$ was prepared at 5GPa. In the HP phase, the parent 1D-$_\infty^1[BiNiO]^{3+}$ *trans* chains of edge-sharing $O(Bi_2Ni_2)$ oxo-centered tetrahedra are conserved but reorganized into a more compact crystal-structure. It returns short Bi-Bi contacts (3.42 Å) with interacting lone pair (LP) electrons via weakly bonding σ bond. The main density of states topology is preserved bringing a calculated bandgap about 3.45 eV for the HP-form against 3.52 eV for the ambient pressure (AP) form. So do the magnetic properties mainly hold by the 1D subunits, which order antiferromagnetically at $T_N = 16.3$ K against 17.5 K in AP-$BiNiPO_5$. Our work attests the oxo-centered polyhedra role and principles, prompt to form the robust framework of the 3D-lattice able to survive structural transformation in extreme conditions.

The large family of bismuth metal (M) phosphate has been intensively investigated during the last decades.[1] The quasi-systematic polymerization of $O(Bi,M)_4$ anti-tetrahedra (A-*Td*) into versatile (0D to 3D) types of structural units is allowed by the flexibility of the A-*Td*s able to co-admit, Bi^{3+} ions, alkali, alkali-earths, transition metals or heavy metals… into more or less ordered frameworks. [2] Among the simplest ordered terms, the $BiMO(XO_4)$ and $BiM_2O_2(XO_4)$ series (M = Ca, Cd, Co, Mg, Mn, Ni, Pb and X = As, P,V) [1] were mainly studied for their optical [3], [4] or magnetic properties. [5]–[8] For instance $BiCu_2O_2(PO_4)$ (BCPO) is a frustrated two-leg S = 1/2 ladder with a cascade of field induced transitions.[9], [10] Recently, high-pressure high-temperature (HP-HT) transformation was used to stabilize a HP polymorph at 5 GPa and 800 °C. In the HP-form, the 1D-ladder topology and spin-gap survive although the effect of the twist between next ladders modify significantly some of the interchain exchanges, see [11].

These results lead us to explore other related systems through the prism of HP-HT route. Here, the concerned $BiMO(XO_4)$ family of compounds was largely detailed in [3]. Their crystal structures display *cis*- or *trans*- 1D oxo-centered $[OBiM]^{3+}$ single-chains built on (OBi_2M_2) A-*Td*s sharing M-Bi (*trans*- case) edges. Only $BiCaVO_5$ [12], [13] and $BiCdVO_5$ [14] have Ca^{2+} and Cd^{2+} in *cis* position which make them singular examples. In any case, the XO_4 surround the chains. Both the *cis*- *vs. trans*- configurations and cationic steric effects for instance of the XO_4 groups (vol. $PO_4 < AsO_4 < VO_4$), may change the crystal symmetry. Most compounds are monoclinic (S.G. $P2_1/n$) [3] (except $BiCaVO_5$ that is orthorhombic, S.G. *Pbca*) becomes triclinic (S.G. *P-1*) in case of big cations (Pb^{2+} or As^{5+} for example), [15], [16] interpretable from chemical pressure effect. Among the series, the M = Ni compound $BiNiPO_5$ (denoted AP-BNPO below, where AP stands for ambient pressure) crystallizes in the $P2_1/n$ space group. [17] Its crystal structure is shown on Fig. 1a with details on the 1D $[OBiNi]^{3+}$ oxo-centered *trans*-chains surrounded by isolated phosphates. A snapshot of the Electron Localization Function (ELF) obtained from DFT calculations, shows evidence of the Bi^{3+} electronic lone pair stereoactivity mainly lying in the *ac* plane in the free interchain space in the AP form.

In the oxo-centered chains, Ni^{2+} cations being in *trans* positions, they share an O-O edge leading to dominant ferromagnetic (FM) Ni-O-Ni super-exchanges (Ni-O-Ni = 99.9 °) well predicted by Kanamori-Goodenough rules.[18] The magnetic structure refined from powder neutron data and the analysis of the magnetic phase diagram confirms that the antiferromagnetic (AFM) ordering below T_N = 17.5 K results for the competition between a large number of inter and intra-chains Ni-O-O-Ni super super-exchanges (SSEs).[5] Keeping this specificity in mind, the HP-HT synthesis route was used to reorder these units HP-BNPO similarly to the AP-BCPO→ HP-BCPO transformation.[11] This paper deals with the HP/HT modification of $BiNiPO_5$, its structural and magnetic investigations and the consequences on Bi-Bi bonding.

Experimental section

Synthesis

Single phase HP-BNPO material was obtained by HP/HT treatment of AP-BNPO at 5 GPa and 600 °C. polycrystalline AP-BNPO was preliminary prepared using the method given in [17] using a stoichiometric mixture of Bi_2O_3, NiO and $(NH_4)H_2PO_4$, treated at 850 °C. The sample was further loaded in a Platinum capsule sealed afterwards and squeezed in a belt-type apparatus system. Details about the press and synthesis conditions are presented in ref [11].

Structural job

Powder X-ray diffraction (XRD) data were collected at room temperature in the range of $2\theta = 5 – 120$ °, with 0.02 step and using a D8 Advance Bruker AXS diffractometer in Bragg Brentano geometry equipped with a 1D LynxEye detector. The Rietveld refinement was performed using JANA2006. [19]

High-Temperature XRD (HT-XRD) was done using a Rigaku SMARTLAB multipurpose diffractometer (9 kW rotating anode) in Bragg–Brentano reflection beam mode (with a PSD 1D detector DTEX) delivering CuKα radiation (λ = 1.5418 Å). High temperature XRD measurements were done loading the sample in an Anton

Paar DHS1100 hot plate stage between room temperature and 850 °C, heating rate 10 °C/min. Omega-2theta scans were performed between 10 ° and 90 ° with a scan speed of 10 °/min.

Magnetic properties

Magnetic data were measured on a Physical Property Measurement System (PPMS) Dynacool (9 T) system from Quantum Design. Typical measurements using zero field cooling (ZFC) and field cooling (FC) procedures were performed at 0.1 T. The Curie Weiss fit was performed in the temperature range of 50 to 300 K. Field dependence of the magnetization was also collected at 2, 50, 100 and 300 K.

Calculation

DFT calculations were performed using the projector augmented-wave (PAW) method [20] implemented in the Vienna ab-initio Simulation Package (VASP) [21], with the full-potential local-orbital scheme (FPLO9.00-33) [22]. We used the generalized gradient approximation (GGA) for electron exchange and correlation corrections [23] applying the local density approximation (LDA + U, U = 7 eV).

The cutoff energy for the plane wave expansion was 550 eV and reciprocal-space integration was performed on dense Monkhorst-pack meshes (21x21x21) for HP-BNPO and (10x14x16) for BNPO-AP. It included 4631 (AP, $P2_1/n$) and 1124 (HP, *P-1*) points in the symmetry-irreducible part of the first Brillouin zone for the crystallographic unit cell. Convergence criteria of 10^{-6} and 10^{-3} were set for convergence of the electronic and cycles and ionic relaxation, respectively. The electronic localization function (ELF) and the density of states of Bi, O and P atoms are deduced from the GGA-only calculations. For bond analysis, after plane-wave DFT calculations, the LOBSTER package [24] allows extraction of the project and Integrated Crystal Orbital Hamilton population p-COHP and I-COHP. Tight Binding Extended Hückel (TBEH) calculations have been performed using the Samoa package. [25]

Results and discussion

Crystal structure

HP-BPNO was found to be stable after releasing first temperature and then pressure. Its XRD pattern (see Fig. S1 in ESI) differs from the one of the AP-BNPO but is reminiscent of the $BiNiO(AsO_4)$ phase / BNAO.[16] It was fully indexed in the triclinic unit cell a = 7.4211(4), b = 6.5606(4), c = 5.1633(3) Å, α = 83.817(2), β = 110.727(2) and γ = 123.412(2) °. The structure was refined in the *P*-1 space group and validates the isomorphism between HP-BNPO and BNAO. We note that similar relationship was established between HP-BCPO and $BiCu_2O_2(AsO_4)$ / BCAO. [11] It is driven by a unit-cell compression by -1.7 % from the AP phase (V_{AP} = 99.17 $Å^3$ vs V_{HPeq} = 97.52 $Å^3$). The Rietveld refinement was performed starting from the BNAO model and further finalized imposing P-O distance restrictions. All oxygen ADP parameters were fixed to 0.012. It results in the final agreement factors R_p= 0.0281, wR_p= 0.0376. The experimental versus calculated XRD patterns are shown on Fig. 1c. The main interatomic distances vary from 2.105 to 2.492 Å for Bi-O, from 1.832 to 2.282 Å for Ni-O and from 1.424 to 1.593 Å for P-O. The atomic coordinates and main distances are gathered in Tables 1 and 2. In Table 1, the refined coordinates are compared to those obtained from DFT-relaxed structure. All the information regarding the refinement are summarized in Table S1 in the ESI. Finally, the crystal structure is shown on Fig. 1b. It is striking that the oxo-centered chains are conserved within nearly-unmodified geometries, which validates their robustness, and principles as rigid structural sub-units. [1] Similar conclusions than in the HP-BCPO study can be proposed. In both cases, the physical pressure compensates the chemical pressure induced by the substitution of P^{5+} by bigger As^{5+} (r_{P5+} - r_{As5+}: 0.17 - 0.33 Å). In that sense, it is possible to foresee the formation of HP-$BiM_2O_2(PO_4)$ and HP-$BiMO(PO_4)$ into crystal structures corresponding to the AP-arsenate polytypes.

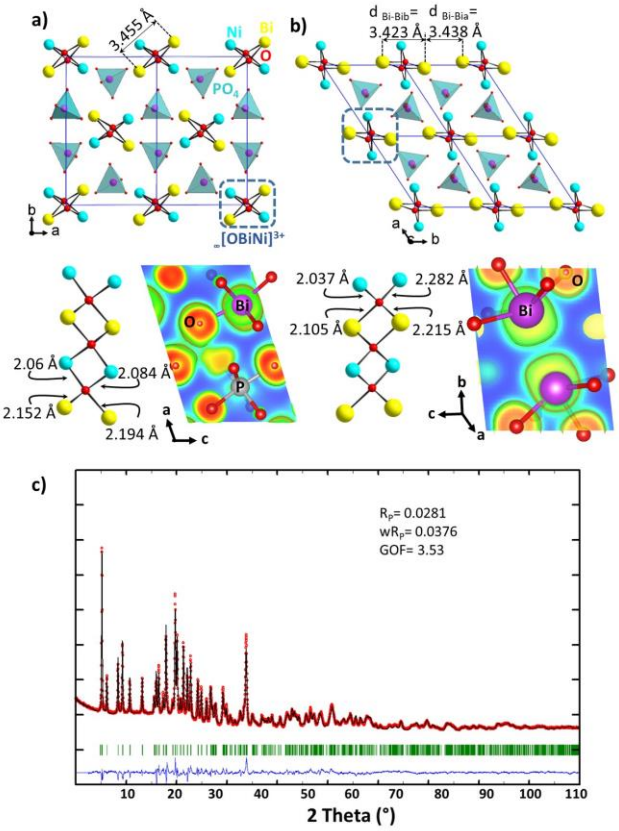

Fig. 1. Projection along the *c*-axis of the a) AP-BNPO, and b) HP-BNPO. Snapshots of the ELF function with evidence of the Bi^{3+} electronic lone pair from DFT calculations for the AP and HP forms of $BiNiO(PO_4)$. The representations were drawn at η(r) = 0.4 isosurface c) Powder XRD Rietveld refinement: the experimental (red) and calculated (black) patterns are superimposed; the difference curve and Bragg positions are respectively represented in blue and green.

Bi-Bi interaction

In the HP-BNPO crystal structure, the Bi-Bi distances between next $[BiMO]^{3+}$ units ($d(Bi\text{-}Bi_a)$ = 3.438(3)) and inside them ($d(Bi\text{-}Bi_b)$ = 3.423(3) Å) are surprisingly almost identical as observed in Fig. 1b), in absence of intermediate $\sigma_{(Bi\text{-}O)}$ bonds for $Bi\text{-}Bi_a$. Here, such "short" Bi-Bi contact mediated by LP electrons pointing towards each other returns an intriguing situation and questions about

the occurrence of a bonding scheme. Indeed, looking at the AP-BNAO isomorph yields a similar situation with even shorter distances of 3.4126(8) Å. [15]

Table 1. Atomic coordinate comparison between Rietveld refinement and relaxed structure from DFT calculation.

Atom				U_{eq}	**BVS**
(Riet)	**X**	**Y**	**Z**		**sum**
(Relaxed)	***X***	***Y***	***Z***		
Bi1	0.9552(3)	0.2302(3)	0.8972(3)	0.0092(5)	2.96(6)
	0.9563	*0.2342*	*0.8956*		
Ni1	0.7250(8)	0.8638(7)	0.3230(9)	0.049(17)	2.11(3)
	0.7270	*0.8669*	*0.3277*		
P1	0.3761(10)	0.6980(11)	0.6492(12)	0.013(2)	5.22(11)
	0.6134	*0.2996*	*0.6642*		
O1	0.926(2)	0.929(2)	0.7331(14)	0.0012	2.26(5)
	0.9545	*0.9503*	*0.7170*		
O2	0.236(2)	0.791(2)	0.614(2)	0.0012	2.27(9)
	0.2101	*0.7765*	*0.6103*		
O3	0.2954(19)	0.4579(12)	0.757(2)	0.0012	2.12(4)
	0.2208	*0.4382*	*0.7411*		
O4	0.458(2)	0.708(2)	0.3990(19)	0.0012	1.74(5)
	0.4261	*0.7025*	*0.3897*		
O5	0.5919(16)	0.8812(16)	0.9002(18)	0.0012	1.90(3)
	0.6129	*0.8811*	*0.4002*		

*U_{eq} oxygen are fixed

Table 2. Typical interatomic distances in HP-BNPO, the DFT-relaxed structures are given in italic.

Atoms		Riet. d, Å *Rel. d, Å*	Atoms		Riet. d, Å *Rel. d, Å*
Bi1	O1	2.105(16) *2.1573*	Ni1	O1	2.037(8) *2.0019*
	O1	2.215(11) *2.3080*		O1	2.282(14) *2.0687*
	O5	2.395(9) *2.3289*		O2	2.165(16) *2.1552*
	O3	2.457(13) *2.3434*		O3	2.107(13) *2.0701*
	O2	2.492(10) *2.4520*		O4	1.833(15) *2.0083*
	O4	3.134(16) *2.9329*		O5	2.073(10) *2.0551*
P1	O2	1.42(2) *1.5736*	P1	O4	1.594(16) *1.5429*
	O3	1.469(10) *1.5549*		O5	1.561(8) *1.5550*
Ni	Ni	3.2533(65) *3.2255*			
Bi	Bib	3.423(3) *3.4019*	Bi	Bia	3.438(3) *3.4656*

The external Bi-Bi contacts are usually longer as compared to most compounds of the Bi_2O_3-MO-X_2O_5 systems in which they are mediated by counter XO_4 groups, or across ionic interleaves (4.5 Å in BiOF) or even across van-der-Waals gap, as for Pb^{2+} in tetragonal PbO (d(Pb-Pb) = 3.84 Å). However, slightly longer Bi-Bi contacts are found in some counter-examples, such as 3.54 Å in $Bi_4MgO_4(PO_4)_2$, see Fig. 2, but interacting [Bi] sublattice is arranged in a compact-shifted manner such that the LP's do not face each other. [26]

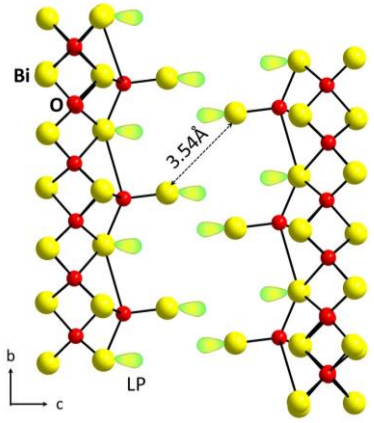

Fig. 2. Long Bi-Bi contacts in $Bi_4MgO_4(PO_4)_2$ with non-facing Bismuth Lone Pairs.

For comparison with anionic or metal Bi more prompt to covalent bonding, this relative short distance across two Bi^{3+} lone pairs in absence of anionic media is longer by 8 % from those found in the naked Bi_2^{4-} anions found in $Ca_{11}Bi_{10}$ (3.15 Å),[27] by 11 % compared to the shortest Bi-Bi bonds in rhombohedral metal bismuth (3.06 Å), [28] by 13 % from the Bi-Bi dimers with single bonds of in the substituted Ph_4Bi_2,[29] and by 19 % from what found in doubly bonded $(Bi_2)^{2-}$ of (K-crypt)$_2(Sn_2Bi_2)$.[30] In a preliminary approach, we better understood the role of the lone pair by calculation of the molecular orbitals (M.O.) by TBEH.[20], for $[BiO_3(PO_4)]^{6-}$ and dimeric $[Bi_2O_6(PO_4)_2]^{12-}$ isolated units, chosen to take into account direct Bi-O and O-P interactions in the first shell of the interacting Bi^{3+} ions.

The role played by anionic ligands in the structural distortion and stereo-activity of the lone-pairs was intensively discussed [32] and finds a major origin from the primary antibonding Bi 6s–O 2p interactions, with Bi 6p orbitals contribution also. This scheme occurs on the HOMO level (assigned to the LP electronic contribution) calculated for monomeric units shown Fig. 3a with strong Bi, s and p contributions. The analysis of the molecular orbital in the dimers is relevant to reveal the Bi---Bi interactions, through bonding σ-type overlaps in the deep core levels, i.e. ~ -9 eV from its antibonding σ*contribution which is the HOMO at the Fermi level. It suggests the creation of weak Bi-Bi interactions, as pictured in the electron localization function (ELF) map shown Fig. 1. Note that in the case of the AP phase, the electronic anisotropy around Bi^{3+} is less pronounced. A more realistic analysis of the complete periodic solid was performed after DFT calculations. Note that the coupling between the electron orbital spin polarized ferromagnetic configuration between Ni^{2+} centers was used, preserving the cell symmetry, with respect to the most important Ni-Ni exchange found FM in the AP-form and expected similar in the HP-one, see below. We did not used spin orbit coupling (SOC) between the electron orbital with its spin moment generated by heavy nuclei, such as bismuth.

The main features of the LDA+U density of states (DOS, Fig. 3b,c) are typical for bismuth transition metal phosphates [4] and conserve the same topology for both the AP and HP-polymorphs. The coordinates deduced from the relaxation are presented in Table 1 and compared with those deduced from the Rietveld refinement.

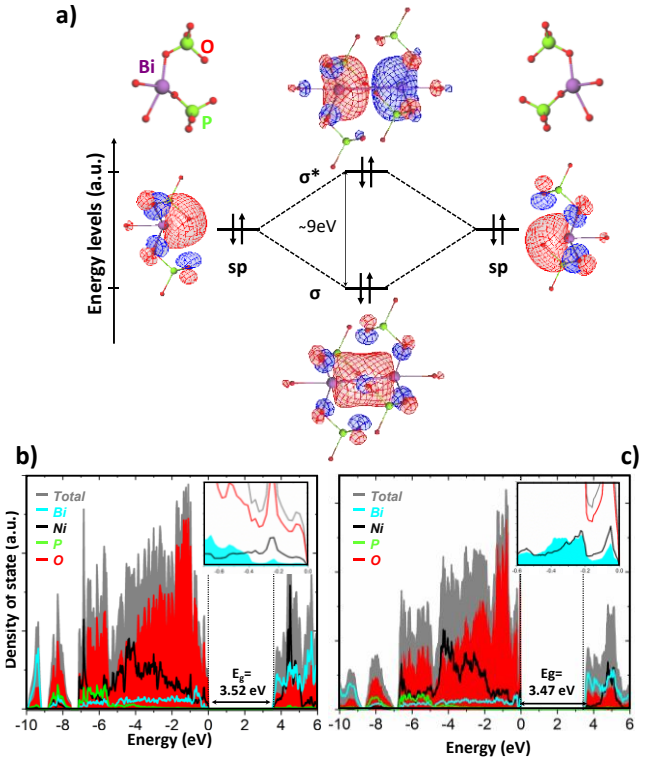

Fig. 3. a) EHTB molecular orbitals for $BiO_3(PO_4)$ and $Bi_2O_6(PO_4)_2$ with creation of σ and σ* levels, total and atomic resolved projected DOS calculated for b) the AP-BNPO and c) the HP-BNPO. The Fermi level is set to 0.

Essentially, the top of the broad valence band (VB) are a mixture of Ni, Bi and O states with small contribution of the P states. These bands lie between ~-7 eV and E_F and account essentially for the bonding within the 1D-chains and with their surrounding oxygen ligands. Only the lowest part of VB shows an appreciable contribution of P *3p* orbitals within the strongly covalent P-O bonds. The magnetic Ni *3d* orbitals lie between -2 eV and unoccupied Ni *d* states, O *2p* and Bi *6p* and *6s* states form the bottom of the conduction band (CB). The compounds presented have very similar bandgap calculated dictated by the similar $[OBiNi]^{3+}$ *trans*-chains. Comparing the Fermi levels (see the insets of Fig. 3b and 3c) of the AP- and HP- forms highlights a sharpest Bi contribution for the HP-polymorph, while Ni d states are found in AP-BNPO. The molecular orbital features found in TBHE are rather well reproduced giving the large Bi contribution around -9 eV (assigned to the bonding (Bi—Bi)$_a$ together with σ*Bi-O levels, and the Bi levels at E_F consistent with the HOMO level which comfort the direct bismuth-bismuth interaction.

After PAW-DFT calculations, we further performed crystal orbital Hamilton population (COHP) analyzes to gauge the nature and bonding strengths in the HP-polytype, focusing on $(Bi\text{-}Bi)_a$ and $(Bi\text{-}Bi)_b$ contacts. Some examples for this process are given in [33], [34]. For a reference, we also calculated the projected COHP (p-COHP) for the shortest Bi-O1 bond of 2.16 Å after ionic relaxation. The Fig. 4 gives the obtained bonding patterns. Bonding and antibonding interactions are represented by negative and positive values of the COHP, while non-bonding return zero values.
For $(Bi\text{-}Bi)_a$, bonding interactions dominate the entire range of valence-bands apart from the strong antibonding region starting 1 eV below the fermi level. This situation is mixed in the $(Bi\text{-}Bi)_b$ case but with much weaker projected-COHP intensities, due to the absence of significant orbital overlap. The cumulative integrated I-COHP values at the Fermi level are -0.89 for the $(Bi\text{-}Bi)_a$ and $(Bi\text{-}Bi)_b$ respectively giving a net bonding capacity for both but strongest through the LP overlap. Comparatively Bi-O1 has a strong covalent bonding character in the full VB giving a superior ICOHP value of -4.2 at E_F. It allows assigning to $(Bi\text{-}Bi)_a$ a weak bonding character, according to the method used here.

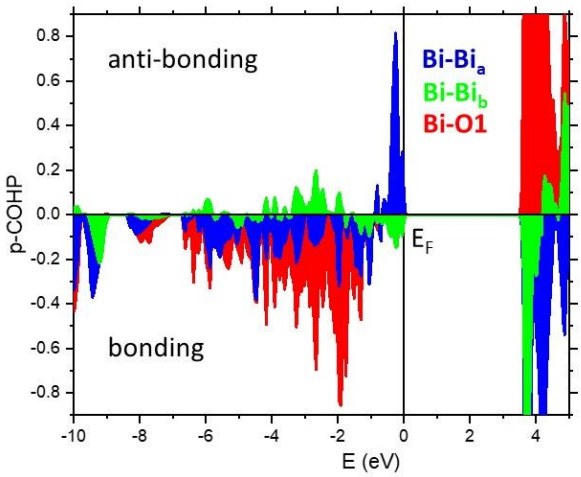

Fig. 4. Crystal orbital Hamilton populations (COHPs) of the HP-BNPO for $Bi\text{-}Bi_a$ (blue), $Bi\text{-}Bi_b$ (green) and $Bi\text{-}O_1$ (red). The Fermi level is set to 0 eV.

HT stability
An *in-situ* X-ray diffraction study versus temperature was performed under air in order to check the stability of the HP-phase. Results are gathered on Fig. 5a, and the evolution of the refined unit cell parameters for both phases are displayed Fig. S2 and S3 in ESI. The HP-form starts to transform back into the AP-form above ~700 °C in air, but remains significant up to 950 °C. Again, this follows the same process largely detailed in [11] and involving a probable 1st order transition, as it led to the co-presence of the two polymorphs in an extended thermal range (Fig. 5b). Plotting the unit cell volume reduced per formula unit as a function of temperature gives two distinct thermal expansion coefficients of $36x10^{-6}$ (HP-BNPO) and $29x10^{-6}$ °C^{-1} (AP-BNPO) respectively (Fig. 5c). However, the V(T) plot of the HP form shows an inflexion around 700 °C, *i.e.* at the HP → AP transformation temperature. Here, $V_{HP\text{-}700°}$ reaches $V_{AP\text{-}RT}$ (see grey arrow on Fig. 5c) where the two forms compete. It is plausible that, up to this point, the internal chemical pressure is relaxed until a 1st order transformation into the AP-form.

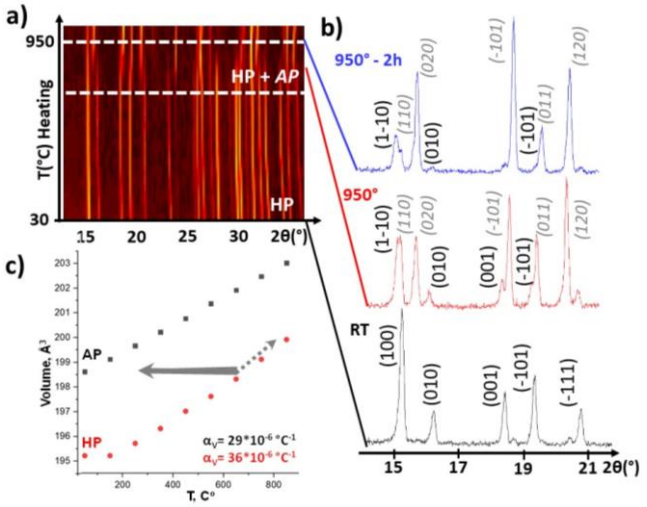

Fig. 5. a) HT-XRD of HP-BNPO. b) Patterns collected at RT (black), at 950 °C (red) and 950 °C after 2h (blue) correspond to HP-BNPO (**hkl** in bold) and HP-AP (*hkl* in italic) mixtures c) plots of the volume per formula unit versus temperature for the two forms. The grey line corresponds to the minimal volume identical between HP and AP forms.

Magnetic properties

The magnetic properties of AP-BNPO were largely detailed in [5] including a magnetic phase diagram function of the relative magnetic exchanges *J*s. From the magnetic structure refined from powder neutron diffraction (PND) the role of the robust ferromagnetically coupled edge-sharing Ni_2O_{10} dimers inside the chains are predominant, while weakest antiferromagnetic inter-dimer super-super exchanges order below T_N = 17.5 K. Due to the preservation of the oxo-centered units in HP-BNPO, the edge-sharing Ni_2O_{10} remains, but significantly distorted see Fig. 6a. It is striking that the Ni-Ni distance is increased under pressure (d_{AP} = 3.1715 Å and d_{HP} = 3.2533 Å) but the Ni-O-Ni angle remain in the orthogonal configuration (Ni-O-Ni_{AP} = 99.87 ° versus Ni-O-Ni_{HP} = 97.58 °) in favor of ferromagnetic exchanges between S = 1 Ni^{2+} ions from Kanamori-Goodenough rules. It leads to very similar magnetic behavior for HP-BNPO, as shown on the χ(T) and χ^{-1}(T)plot of Fig. 6b. It shows a paramagnetic regime above T_N = 16.7 K, characterized by a Curie Weiss law $\chi = C/(T-\theta_{CW})$ with θ_{CW} = -28.0 K and μ_{eff} = 3.29 μ_B/Ni^{2+} which denotes a significant but rather common orbital contribution. Here again from Goodenough Kanamori rules the exchanges inside the dimers are expected FM. The mean field approach allows estimation of the mean inter-chain exchanges, using $\theta_{CW} = \Sigma_i z_i S(S+1) J_i/3K_b$, where S = 2 for FM Ni_2O_6 dimers and Z = 12 is the number of connected neighbors by SSEs, see Fig. S4 in ESI for additional representations. It leads to J_{inter}/K_b = -1.16 K. Compared to AP-BNPO (θ_{CW} = -11.5 K, Z=14) the J_{inter}/Kb value of -0.41 K is well scaled by Ni-Ni interatomic distances in the compact HP-BNPO (4.7 to 5.6 Å along the SSE paths against 5.2 to 5.7 Å for AP-BNPO. The M(H) plots at various temperatures, displayed Fig. 6c, show a robust antiferromagnetic state M = 0.28 μB/FU at 2 K. A slight deviation from linearity at $\mu_0.H_c$ = 6 T suggest a slight metamagnetic accident probably by surpassing one of the multiple J inter between FM-dimers. We note that according to the energy of a spin in a magnetic field H given by g.H.μ_B.S (where the Landé factor g ~2, μB = 0.672 J/T and S = 2 for robust spin dimers), we found and energy of ~16 K close to the T_N at zero-field. It validates a specific magnetic transition at Hc with emphasized alignment of S = 2 macro spins along the external field.

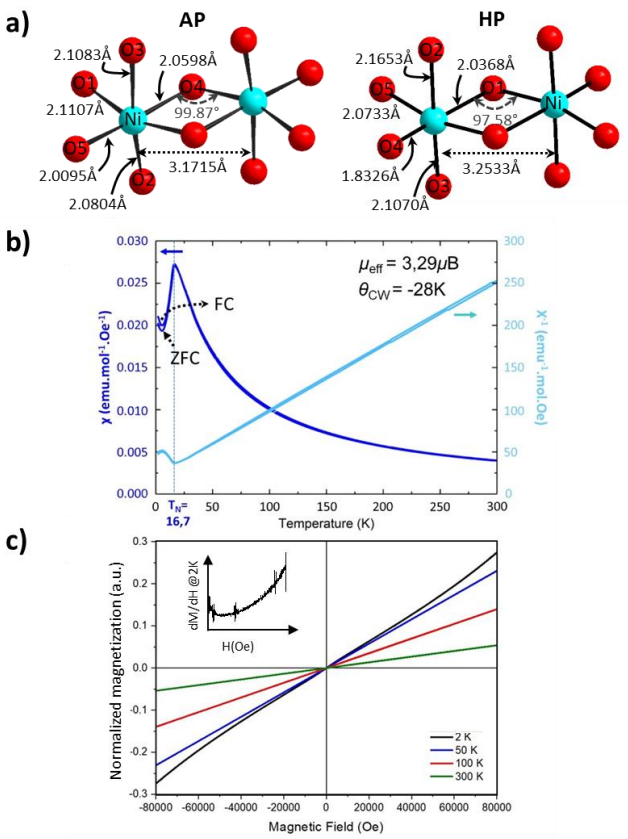

Fig. 6. a) Structural evolution of dimers between AP and HP-BNPO, b) ZFC-FC magnetic susceptibility (dark blue) and inverse susceptibility (light blue) of HP-$BiNiPO_5$ as a function of temperature. The magnetic field is set to 0.1 T c) field dependence of the magnetization of HP-$BiNiPO_5$ at selected temperatures, and in insert, its derivative at 2 K.

Conclusion

To summarize, similarly to HP-BCPO, [11] HP-BNPO prepared at 600 °C and P = 5 GPa adopts the crystal structure of the arsenate variant BNAO. The chemical pressure drop after replacement of AsO_4 by smaller PO_4 is compensated by physical pressure and allows to stabilized this metastable form. The creation of short weakly bonding Bi^{3+}---Bi^{3+} contacts were examined by Tight binding Hückel and Crystal orbital Hamilton populations analysis. Upon heating the pressure is relaxed until the volume of the AP-form is reached, returning a plausible 1st order HP-BNPO → AP-BNPO transition around 700 °C. Such chemical pressure compensation by high pressure route opens a wide route towards the prediction and stabilization of new tailor-made materials, in various chemical systems. According to the structural analogy between the

HP and AP variants, it is striking that the robust preserved structural units are hold by oxo-centered principles. [1]

ASSOCIATED CONTENT

Supporting Information

The Supporting Information is available free of charge on the ACS Publications website xxxx at DOI: xxxx.

Materials preparation, characterization methods, computational details, Rietveld refinements and EDS analysis.

AUTHOR INFORMATION

Corresponding Author

* E-mail: Marie.Colmont@centralelille.fr

Author Contributions

The manuscript was written through contributions by all authors.

Notes

The authors declare no competing financial interests.

ACKNOWLEDGMENT

The Fonds Européen de Développement Régional (FEDER), CNRS, Région Nord Pas-de-Calais, and Ministère de l'Education Nationale de l'Enseignement Supérieur et de la Recherche are acknowledged as well as the X-Press team from Institut Néel (Murielle Legendre and Céline Goujon).

REFERENCES

[1] S. V. Krivovichev, O. Mentré, O. I. Siidra, M. Colmont, et S. K. Filatov, *Chem. Rev.*, 2013, **113**, 6459-6535.

[2] M. Lü, A. Aliev, J. Olchowka, M. Colmont, M. Huvé, C. Wickleder and O. Mentré, *Inorg. Chem.*, 2014, **53**, 12058-12065.

[3] J. Olchowka, M. Colmont, H. Kabbour, and O. Mentré, *J. Alloys Compd.*, 2017, **709**, 373-380.

[4] J. Olchowka, O. Mentré, H. Kabbour, M. Colmont, M. Adlung, M. Suta and C. Wickleder, *Chem. - Eur. J.*, 2017, **23**, 15694-15703.

[5] O. Mentre, F. Bouree, J. Rodriguez-Carvajal, A. El Jazouli, N. El Khayati, et E. M. Ketatni, *J. Phys. Condens. Matter*, 2008, **41**, 415211.

[6] B.-G. Jeon, B. Koteswararao, C.B. Park, G.J. Shu and S.C. Riggs, *Sci. Rep.*, 2016, **6**, nº 1.

[7] O. Mentré, E. Janod, P. Rabu, M. Hennion, F. Leclercq-Huge, J. Kang, C. Lee, M.H. Whangbo and S. Petit, *Phys. Rev. B*, 2009, **80**, 180413.

[8] O. Mentré, E. M. Ketatni, M. Colmont, M. Huvé, F. Abraham, et V. Petricek, *J. Am. Chem. Soc.*, 2006, **128**, 10857-10867.

[9] Y. Kohama, S. Wang, A. Uchida, K. Prsa, S. Zvyagin, Y. Skourski, R.D. McDonald, L. Balicas, H.M. Ronnow, C. Rüegg, M. Jaime, *Phys. Rev. Lett.*, 2012, **109**, nº 16.

[10] Y. Kohama, K. Mochidzuki, T. Terashima, A. Miyata, A. DeMuer, T. Klein, C. Marcenat, Z.L. Dun, H. Zhou, G. Li, L. Balicas, N. Abe, Y.H. Matsuda, S. Takeyama, A. Matsuo and K. Kindo, *Phys. Rev. B*, 2014, **90**, nº 6.

[11] M. Colmont, C. Darie, A. A. Tsirlin, A. Jesche, C. Colin, et O. Mentré, *Inorg. Chem.*, 2018, **57**, 6038-6044.

[12] J. Boje et Hk. Müller-Buschbaum, *Z. Für Anorg. Allg. Chem.*, 1993, **619**, 521-524.

[13] Z. Pei, A. van Dijken, A. Vink, et G. Blasse, *J. Alloys Compd.*, 1994, **204**, 243-246.

[14] I. Radosavljevic, J. A. K. Howard, et A. W. Sleight, *Int. J. Inorg. Mater.*, **2000**, 543-550.

[15] X. Xun, A. Yokochi, et A. W. Sleight, *J. Solid State Chem.*, 2002, **168**, 224-228.

[16] A. C. Roberts, P. C. Burns, R. A. Gault, A. J. Criddle, M. N. Feinglos, et J. A. R. Stirling, *Eur. J. Mineral.*, 2001, **13**, 167-175.

[17] Ketatni M., Abraham F., et Mentre O., *Solid State Sci.*, 1999, 449-460, 1999.

[18] J. B. Goodenough, *Magnetism and the chemical bond*. Huntington, N.Y.: R. E. Krieger Pub. Co, 1976.

[19] V. Petříček, M. Dušek, et L. Palatinus, *Z. Für Krist. - Cryst. Mater.*, 2014, **229**, 1737.

[20] P. E. Blöchl, *Phys. Rev. B*, 1994, **50**, 17953-17979.

[21] Kresse, G. et J. Furthmüller, « Vienna Ab-initio Simulation Package (VASP) ». 2012.

[22] K. Koepernik et H. Eschrig, *Phys. Rev. B*, 1999, **59**, p. 1743-1757.

[23] J. P. Perdew, K. Burke, et M. Ernzerhof, *Phys. Rev. Lett.*, 1996, **77**, 3865-3868.

[24] S. Maintz, V. L. Deringer, A. L. Tchougréeff, et R. Dronskowski, *J. Comput. Chem.*, 2016, **37**, 1030-1035.

[25] D. Dai, J. Ren, W. Liang, et M. H. Whangbo, « SAMOA (Structure and Molecular Orbital Analyzer) program package », 2002. http://chvamw.chem.ncsu.edu/

[26] D. Endara, M. Colmont, M. Huvé, G. Tricot, L. Carpentier, et O. Mentré, *Inorg. Chem.*, 2012, **51**, 4438-4447.

[27] M. Sturza, F. Han, C. D. Malliakas, D. Y. Chung, H. Claus, et M. G. Kanatzidis, *Phys. Rev. B*, 2014, **89**, 054512.

[28] P. Cucka et C. S. Barrett, *Acta Crystallogr.*, 1962, **15**, 865-872.

[29] F. Calderazzo, R. Poli, et G. Pelizzi, *J. Chem. Soc. Dalton Trans.*, 1984, **11**, 2365.

[30] S. C. Critchlow et J. D. Corbett, *Inorg. Chem.*, 1982, **21**, 3286-3290.

[31] S. Wang, D. B. Mitzi, G. A. Landrum, H. Genin, et R. Hoffmann, *J. Am. Chem. Soc.*, 1997, **119**, 724-732.

[32] J. Yang et M. Dolg, *Phys. Chem. Chem. Phys.*, 2007, **9**, 2094.

[33] W.-L. Li, C. Ertural, D. Bogdanovski, J. Li, et R. Dronskowski, *Inorg. Chem.*, 2018, **57**, 12999-13008.

[34] S. Steinberg et R. Dronskowski, *Crystals*, 2018, **8**, 225.